INTERFACE

rsif.royalsocietypublishing.org

Research

Cite this article: Karakasiliotis K, Thandiackal R, Melo K, Horvat T, Mahabadi NK, Tsitkov S, Cabelguen JM, Ijspeert AJ. 2016 From cineradiography to biorobots: an approach for designing robots to emulate and study animal locomotion. *J. R. Soc. Interface* **13**: 20151089. http://dx.doi.org/10.1098/rsif.2015.1089

Received: 20 December 2015
Accepted: 2 June 2016

Subject Category:
Life Sciences–Engineering interface

Subject Areas:
biomimetics, computational biology

Keywords:
robotics, salamander, amphibious, cineradiography

Author for correspondence:
R. Thandiackal
e-mail: robin.thandiackal@epfl.ch

Electronic supplementary material is available at http://dx.doi.org/10.1098/rsif.2015.1089 or via http://rsif.royalsocietypublishing.org.

THE ROYAL SOCIETY PUBLISHING

From cineradiography to biorobots: an approach for designing robots to emulate and study animal locomotion

K. Karakasiliotis[1], R. Thandiackal[1], K. Melo[1], T. Horvat[1], N. K. Mahabadi[1], S. Tsitkov[1], J. M. Cabelguen[2] and A. J. Ijspeert[1]

[1]Biorobotics Laboratory, École Polytechnique Fédérale de Lausanne, 1015 Lausanne, Switzerland
[2]Institut National de la Santé et de la Recherche Médicale (INSERM) U 1215-Neurocentre Magendie, Université de Bordeaux, Bordeaux Cedex, France

Robots are increasingly used as scientific tools to investigate animal locomotion. However, designing a robot that properly emulates the kinematic and dynamic properties of an animal is difficult because of the complexity of musculoskeletal systems and the limitations of current robotics technology. Here, we propose a design process that combines high-speed cineradiography, optimization, dynamic scaling, three-dimensional printing, high-end servomotors and a tailored dry-suit to construct Pleurobot: a salamander-like robot that closely mimics its biological counterpart, *Pleurodeles waltl*. Our previous robots helped us test and confirm hypotheses on the interaction between the locomotor neuronal networks of the limbs and the spine to generate basic swimming and walking gaits. With Pleurobot, we demonstrate a design process that will enable studies of richer motor skills in salamanders. In particular, we are interested in how these richer motor skills can be obtained by extending our spinal cord models with the addition of more descending pathways and more detailed limb central pattern generator networks. Pleurobot is a dynamically scaled amphibious salamander robot with a large number of actuated degrees of freedom (DOFs: 27 in total). Because of our design process, the robot can capture most of the animal's DOFs and range of motion, especially at the limbs. We demonstrate the robot's abilities by imposing raw kinematic data, extracted from X-ray videos, to the robot's joints for basic locomotor behaviours in water and on land. The robot closely matches the behaviour of the animal in terms of relative forward speeds and lateral displacements. Ground reaction forces during walking also resemble those of the animal. Based on our results, we anticipate that future studies on richer motor skills in salamanders will highly benefit from Pleurobot's design.

1. Introduction

Agile locomotion in animals results from a complex interplay of various components, involving: the central nervous system, the peripheral nervous system, the musculoskeletal system and interactions with the environment [1]. This makes decoding the mechanisms of locomotor control a difficult problem. Researchers have been trying to determine the role of each component with different approaches: (i) locomotion studies involving kinematic and dynamic recordings [2], (ii) electromyographic studies [3], (iii) neurophysiological studies *in vitro* and *in vivo* [4], (iv) electrical stimulation studies [5] and more. In addition to animal experiments, computational and robotic studies can be very useful in investigating interactions between the different components [6–8]. 'Robots have multiple properties to complement animal studies: their actions are repeatable, they offer access to variables or quantities that would be difficult to measure on animals, they can perform movements that are unnatural or dangerous for animals, and their morphology can be systematically changed' [8]. Used as the physical models of animals, robots are interesting as complements to neuromechanical simulations because they provide real physics. This is particularly

important for locomotion that relies on complex interactions with the environment, such as swimming, crawling on mud, etc., because the motions involved are very difficult to simulate properly. Biorobots are therefore increasingly used as tools in locomotion studies to test hypotheses about biomechanics and neural control (see [8] for a review). There are several examples of studies [9–13] in which robots have been instrumental in understanding some properties of animal locomotion.

Two approaches can be distinguished among computational and physical models: template and anchor models [14]. 'A template is the simplest model (least number of variables and parameters) that exhibits a targeted behaviour'. An anchor is 'a more realistic model fixed firmly or grounded in the morphology and physiology of an animal'. Templates are useful for studying the general principles of locomotion. The same template model can represent several types of animals, such as the spring-loaded inverted pendulum (SLIP) model for legged running [15]. Physical models (i.e. robots) have been designed based on template models, for instance the biped ATRIAs robot [16], the hexapod RHex robot [17] and the salamander-like Salamandra robotica [10]. These robots were designed to use the lowest number of degrees of freedom (DOFs) to obtain and study a particular type of locomotion. Depending on the specific targeted behaviour, template models can be made as complex as necessary (but not more). Anchor models can then be used to validate the templates and to analyse multi-leg coordination, joint torques and neuromechanical aspects.

Salamanders have attracted the attention of researchers from various fields. In particular, they have garnered the interest of neuroscientists for investigating the neural mechanisms that produce their various aquatic and terrestrial locomotor modes as well as the cellular and molecular mechanisms underlying their impressive regenerative abilities [18–21]. Moreover, because salamanders resemble the early tetrapods in their skeletal morphology and locomotor modes more than any other extant species [22–32], they can be used as experimental models to obtain some insight into the neural mechanisms underlying aquatic-to-terrestrial transition in primitive tetrapods [10]. We are currently investigating the interplay between central pattern generation, sensory feedback and descending modulation for producing the large variety of motor behaviours involving whole-body movements as exhibited by salamanders. In previous work [10], we designed a simple template robot model of the salamander with a central pattern generator (CPG) model that could generate two motor behaviours of the salamander (swimming and walking trot) and that included two descending pathways (left–right stimulation). However, the salamander is capable of producing a larger variety of motor behaviours and is known to have more descending pathways. This motivated the design of an anchor model of the salamander. So far, we have mainly explored two descending pathways (left–right stimulation) but more pathways exist in the salamander. In the neural models, additional descending pathways can be added to stimulate subparts of the complete locomotor circuit (e.g. only the tail, only the hind left limb) similar to the action of strings in a marionette. The way in which specific behaviours are generated, when only the marionette is visible but not its strings, can be inferred from a model. The better the model captures the DOFs of the marionette, the closer one can estimate the number of strings needed for the model to reproduce the observed behaviours. In the same way, if the behaviour of the marionette depends on external interactions, then one has to be able to simulate those interactions with the model. Capturing those interactions accurately, especially when they cannot be properly simulated, is important and, for that reason, a physical model—in our case, a salamander-like robot—is necessary. It is important to try to include all the components that influence locomotion: the spinal cord circuits, the sensory feedback, the descending modulation, the internal body dynamics (i.e. muscle dynamics, the musculoskeletal dynamics) and the external body–environment dynamics. Locomotion will likely never be completely understood without investigating the interaction of all these components (i.e. while necessary, it is not sufficient to investigate these components in isolation). At the same time, we realize that any of these components will only be approximations, and future work will involve investigating the effect of these approximations, for instance by comparing the results of experiments carried out with components implemented at different levels of abstraction, e.g. coupled oscillator models versus spiking neural network models for the spinal circuits [33], and different types of muscle models.

Our previous robots, Salamandra robotica I and II, were designed to investigate the transition between swimming and walking [10,34]. Those robots have 10 and 12 actuated DOFs, respectively, and use simple one DOF rotational limbs like the RHex robot [17] for ground locomotion. They can be seen as template models with just the minimal number of DOFs to investigate interlimb and body–limb coordination in steady-state swimming and walking gaits. However, the limited number of DOFs not only restricts our ability to study the organization of the limb CPG networks, but also prevents the study of richer motor skills (e.g. aquatic stepping gaits, turning, paddling, etc.) where multiple DOFs are used [35,36]. For example, we showed in previous work [34,37] that a single rotational DOF at each limb is a limiting factor for understanding turning in salamanders and discussed the importance of a knee joint. It is also easy to show that for aquatic stepping and paddling single-DOF limbs cannot capture the necessary interactions with the environment (e.g. regulating the distance between the feet and the girdles, so that traction with the ground is maintained, or orienting the limb in such way that the hydrodynamics are similar to the ones that the animal experiences).

Building an anchor robot involves multiple design challenges: (i) designing the proper kinematic structure, i.e. the topology and number of DOFs, capable of emulating the desired animal behaviours, (ii) matching similar dimensions and mass distributions, and (iii) replicating muscle-like properties and more generally viscoelastic properties of the body. However, even in anchor models, many trade-offs and simplifications need to be made. The constraints relate to technological limitations in actuation (size, weight, torque, power density and velocity limits) and sensing (size and accuracy), price and manufacturability which highly affect the accessibility of the platform to various researchers as well as studies of morphological variability. Variations of the optimized platform—possibly, but not necessarily, drawn from the variability found in salamanders and other sprawling animals—will give hints on the role of body morphology with respect to the organization of the locomotor network and the pathways that regulate it.

Here, we present an approach to design a biorobot as an anchor model and use it to create Pleurobot, an amphibious salamander-like robot that emulates *Pleurodeles waltl* (*P. waltl*). Key elements of Pleurobot's design are the number and

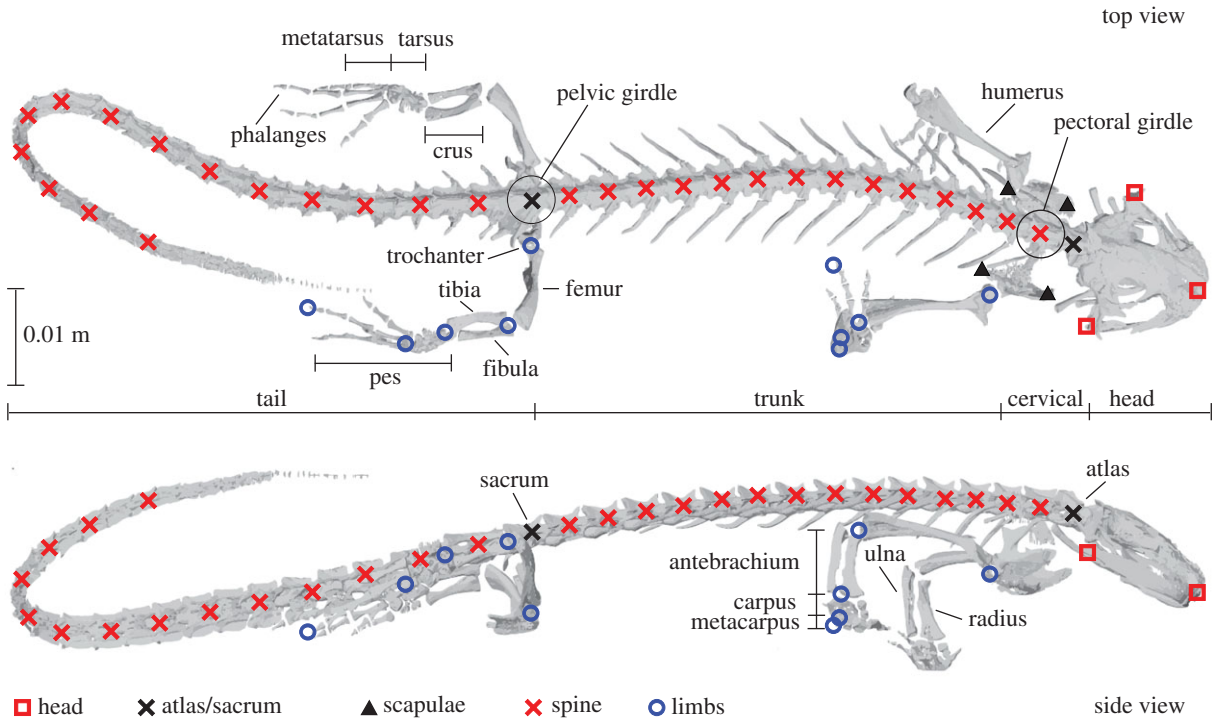

Figure 1. *Pleurodeles waltl* skeletal system. The basis of the design methodology is built from a careful analysis of cineradiographic recordings, the subsequent tracking of the bone structure and the three-dimensional reconstruction. Top and side view of a CT scan are shown, where the markers indicate tracked points: three points for the head, four points for the scapulae, five points for each limb, 16 points in the trunk and 20 points in the tail were included in the analysis. The sacrum was used to separate between trunk and tail.

placement of locomotion-relevant joints. Our approach is then composed of the following steps: (i) collecting three-dimensional kinematics of skeletal elements using biplanar high-speed cineradiography; (ii) optimization of the robot kinematic structure using a genetic algorithm (GA) to be able to replay the set of collected gaits; (iii) dynamic scaling, i.e. performing an analysis of the animal and robot dynamics to ensure that the animal and robot gaits are carried out within the same regimes of interaction forces with the environment; (iv) constructing the robot using three-dimensional printed parts, high-end servomotors and a tailored dry-suit; and (v) comparing the robot and animal gaits with motion capture and force plate measurements. The main features compared with previous design methods are the combination of cineradiography and optimization to identify important locomotion-relevant DOFs for making the robot structure that can easily change depending on the hypothesis being tested. Cineradiography, in our case biplanar, is increasingly used to characterize animal locomotion [38,39]. In biorobotics, it has been used to compare animal and robot locomotion, e.g. during sand swimming [11], or to extract design principles for template-like robots [40] or robot simulations [41], but to the best of our knowledge, it has not yet been used together with optimization algorithms to design a physical anchor-like robot model. An important feature that makes *P. waltl* an excellent animal to model is its low dynamic behaviours, especially during ground locomotion. Many of the skills that can enrich our understanding of the salamander's locomotor network are much less dynamic than other animals, like mammals for instance. Our methodology is based on this fact. Not only current technology reaching its limits in producing reliable dynamic platforms, but also muscle, tendon and bone properties become much more important during dynamic locomotion.

2. Pleurobot's design methodology and development

Our robot is based on *P. waltl*, a salamander that exhibits both terrestrial and aquatic locomotion. This salamander represents a good candidate for our design approach, having been subject to neurophysiological [19,42], electromyographic [43] and biomechanical [10,36] studies in the past. Its morphology is composed of an elongated body (trunk and tail) and four limbs located at the pectoral and pelvic girdles (figure 1). The average body length and weight of *P. waltl* specimens ($n = 2$, 8.45 ± 0.078 cm snout–vent length, SVL) considered for this study were approximately 17.6 cm and 23.8 g. Biplanar high-speed cineradiographic (Neurostar® Siemens AG) recordings at 500 fps and image resolution of 1536×1024 were performed at the University of Jena, Germany. The data presented here have been partially published elsewhere [36] and in detail in a doctoral thesis [44]. More specifically, walking gaits have been described in [36], whereas the data for aquatic stepping and swimming are original. A comparison between animal and robot sizes is provided in table 1.

As discussed in Introduction, several constraints guide the design of an anchor robot. Some are related to technology, and some are driven by the designer's goals. For Pleurobot, we consider one of the most important constraints to be the ability to easily produce copies and variations of the robot at a reasonable price and time, while still being able to test hypotheses on rich motor skills. Most of the rich behaviours of the salamander depend on its segmented limbs (turning, paddling and more), so particular focus was given in replicating the DOFs of the limbs. An important technological constraint is actuation. Currently, the most accessible, efficient and

Table 1. Comparison of animal and robot dimensions.

characteristic length	*P. waltl*	Pleurobot
snout–vent length (m)	0.085	0.73
body length (m)	0.176	1.52
mass (kg)	0.024	7.40
scaling factor (−)	1	8.6

cost-effective actuator is the DC motor. However, DC motors still remain inefficient in very small scales, and we had to choose larger DC motors than we would have liked. Therefore, the motors' size guides the robot's final size, which is larger than the animal (table 1). Given these constraints, the key element of Pleurobot's design is to determine two important engineering considerations: (i) the number of locomotion-relevant joints and (ii) the placement of each joint along the robot's body.

Therefore, we developed a dataset of sequential whole-body postures for walking, swimming and aquatic stepping using the cineradiographic recordings and the three-dimensional reconstruction of kinematics obtained from experiments with *P. waltl*. In order to derive the three-dimensional reconstruction from the cineradiographic recordings, the salamander skeleton was manually tracked in all the videos where the animals showed straight and steady-state locomotion. For this purpose, a custom software based on OpenCV (open graphics C/C++ library) was developed and used. The top and side views were digitized at a frame rate of 40 Hz for swimming and 80 Hz for walking. The dataset of body postures was then used to guide an optimization problem with two goals: (i) optimal segmentation of the robot, i.e. minimum number of joints and (ii) their optimal placement, so that the segmented body can reproduce recorded animal postures in our dataset. The spine, forelimbs and hindlimbs were optimized as three separate kinematic chains.

2.1. Spine

The cineradiographic data for the axial movements of the salamander show that during steady-state locomotion (both in walking and swimming gaits), salamanders undulate mainly in the transverse (horizontal) plane; bending in the sagittal (vertical) plane was almost constant [36,44]. This reduced the problem of designing the robot spine to its optimal segmentation in the transverse plane.

Each snapshot of the salamander spine was represented as a continuous curve in the transverse plane (figure 2*a*,*b*). The mean length of all the curves in the dataset was used to define the length of the segmented line that represents the spine of the robot (including head). Note that the length we refer to here represents part of the animal's spine, in particular 79% of the body length. The remaining 21% (end of the tail) presented rather irregular kinematics between cycles, suggesting that mostly passive dynamics shape the end of the tail during walking or swimming (figure 2*c*).

We performed several optimization runs with different predefined numbers of joints using a GA.[1] Having the craniocervical joint (i.e. neck joint) fixed, the position of each of the other joints was open for optimization. Arbitrarily, 3–15 joints were used in different optimization runs (figure 2*d*). The GA generated new positions for the corresponding number of joints at each iteration. To evaluate how well the given joints and their positions could reproduce the curvature of the salamander's spine, we introduced an error metric as the sum of squared areas between the segmented line and each curve found in the dataset of animal postures (figure 2*e*). This was done for 80 trials, which corresponds to a total of 2798 analysed postures both in water and on the ground. For each specific number of joints, the optimal positions were assumed when the fitness function converged to a very small value (10^{-6}). For the GA in our spine optimization of the robot, we used the GA implementation from Matlab (Matlab 2014b) with default parameters. As such, we used the following parameters: a population size of 200, a crossover fraction of 0.8 and a migration fraction (guarantees survival from one to the next generation) of 0.05.

As expected, the greater the number of joints, the better the segmented line can capture the shapes of the animal's spine during locomotion (figure 2*d*). The approximately exponential convergence of the total error value allowed us to arbitrarily select 10 joints which we considered as a good trade-off based not only on the geometry, but also on the resulting length of the robot. Including the craniocervical joint, which makes a total of 11 spine joints (figure 3*a*). This number and their corresponding optimal positions allow Pleurobot to imitate the bending of the salamander's spine in different gaits to a good extent as illustrated in the accompanying videos and discussed below. Note in figure 3*b* and table 2 how the optimization found that a higher curvature is needed around the hind but not around the front girdle. This is a result of both the limited bending of the front part of the body for all gaits [36] and the increasing curvature of the spine towards the tail during swimming. Two passive DOFs (green in figure 3*a*) were placed at the first and the last segment of the tail to account for the passive bending of the salamander's tail in the sagittal (vertical) plane. It is important to note here that this partially optimal segmentation, guided by a subset of the behaviours observed in salamanders, might prove less optimal for behaviours for which data are not yet available and were not used in the optimization. However, we strongly believe that except for turning gaits, most other behaviours are based on either walking or swimming patterns or a mix of the two (e.g. underwater stepping or paddling). Future experiments will show whether Pleurobot's 'optimal' design captures turning gaits poorly, in that case the ease of producing variations in the robot design will prove significant.

2.2. Limbs

The hindlimb of the salamander consists of two main segments (figure 1), the thigh and the crus. In [36], we described those two segments as a four DOFs manipulator with three DOFs at the hip joint and one at the knee. The analysis of the kinematics suggested that all four DOFs are used during locomotion and they were therefore all included in Pleurobot. Adjoining the two main segments is the foot, which has a highly complex structure with compliant elements as well as bones. While, in our future work, we plan to use Pleurobot to demonstrate the principles of sprawling locomotion with biomimetic feet, we consider the feet here as simple point-contact elements. We discuss the effects of simplifying the foot structure in the experimental validation of Pleurobot (§5). In all walking trials, salamanders clearly showed foot ground contact at the

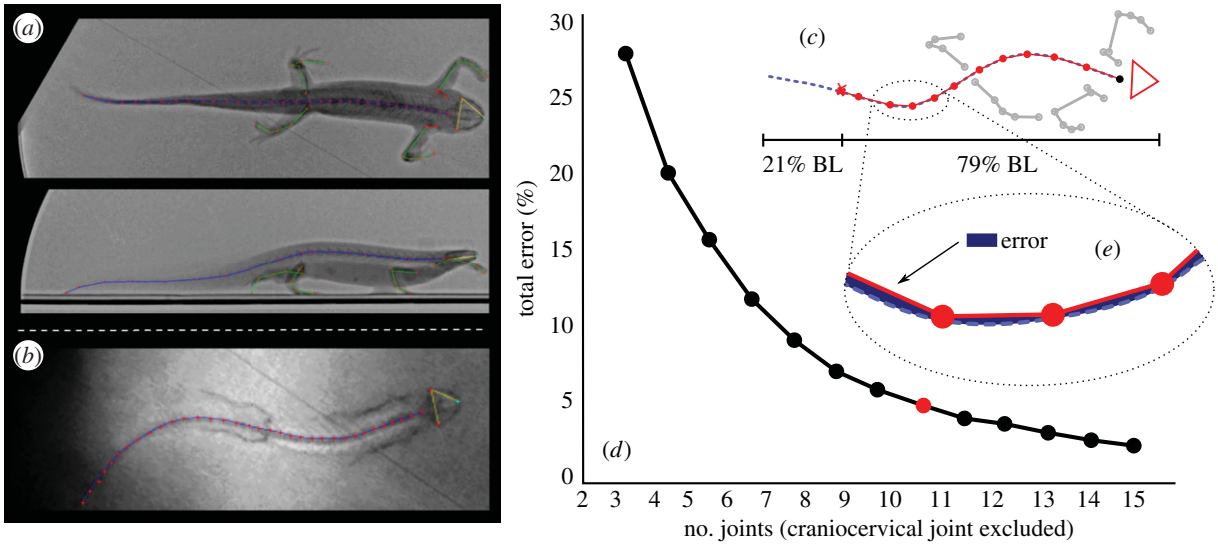

Figure 2. Spine optimization based on the cineradiographic data. We used the cineradiographic recordings of *P. waltl* and the resulting three-dimensional kinematics of the skeletal structure to design the robot's spine: (*a*) top and side view snapshots for walking and (*b*) top view for swimming. The markers indicate which points were tracked. Assuming mostly constant bending in the sagittal plane, the spinal movements in the transverse plane were approximated by a segmented spine (*c*) (BL, body length). The segmentation was derived via an optimization procedure (*d*), in which separate optimizations for various numbers of joints were carried out. For each joint configuration, the segment lengths were derived via an optimization using a genetic algorithm (GA). The error area (*e*) between observed spinal bending in *P. waltl* and the segmented line was used as a fitness function. A resulting number of 10 joints (red data points) was chosen as a trade-off between accuracy of the approximation and a minimal number of joints.

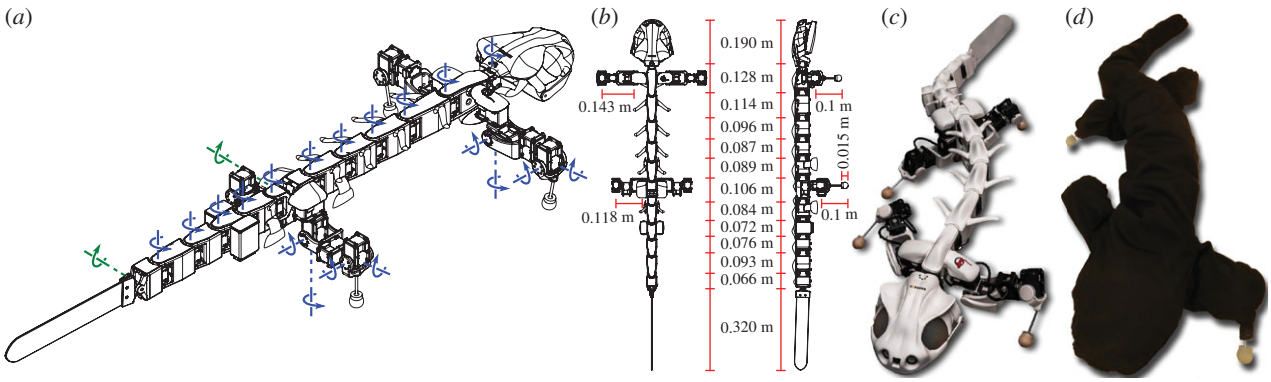

Figure 3. Pleurobot. Following our design methodology, Pleurobot with a total of 29 degrees of freedom (DOFs) was derived. In (*a*), blue axes indicate the 27 motorized DOFs, whereas the green axes indicate two passive DOFs (i.e. unactuated free joints). The results from the spine optimization together with segmented limbs (*b*), allow replicating various gaits, such as walking, swimming and aquatic stepping. The robot design (*c*) comprises three-dimensional printed parts (white), 27 off-the-shelf servomotors (black), silicon feet and a flexible tail. (*d*) A waterproof swimming suit out of a Lycra® Nylon fabric laminated with a 1 mm layer of polyurethane completes the design that allows locomotion in terrestrial as well as aquatic environments.

metatarsals, i.e. at the distal region of the foot. For that reason, Pleurobot's ball-foot element was placed at the mean distance of the metatarsus to the animal's knee during locomotion.

Consequently, the robot's limbs consist of a two-link system with the hip approximated by three consecutive DOFs and a one-axis knee joint. Pleurobot's forelimbs and hindlimbs follow the same design methodology, whereas their corresponding element sizes were measured and scaled up from the animal's CT scan. Excluding the feet and some possible structural elasticities in the animal's joints, it is reasonable to say that Pleurobot's limbs are a closely scaled up replica of the animal's limbs.

2.3. Hardware implementation

For the actuation, we chose Dynamixel MX-64R servomotors from ROBOTIS, Inc., as they offer a good trade-off featuring a fairly high torque-mass ratio (7.3 Nm of stall torque at 126 g), maximum no-load speed of 78 rpm and positional accuracy (0.088° resolution) at a reasonable price. The locomotion controller for replicating the animal gaits is implemented on an Intel Atom 1.6 GHz-based computer provided by ROBOTIS (DW-EK01) placed inside the robot head. The same hardware kit handles the low-level communication with the servomotors through an RS-485 bus at 1 Mbps. We were able to send position commands to the servomotors at a rate of 1 kHz. The entire mechanical structure of Pleurobot is created using three-dimensional printing (Laser sintering), using three variations of polyamide 12 (plastic): the skull (head) is made out of natural polyamide, the spinal segments are made out of glass-filled polyamide and the limb segments out of aluminium-filled polyamide. The two main meta-materials were used because of their increased strength compared with natural polyamide, and also because of the higher density

Table 2. Pleurobot segment dimensions.

segment	length (m)
head	0.190
joint 1–joint 2	0.128
joint 2–joint 3	0.114
joint 3–joint 4	0.096
joint 4–joint 5	0.087
joint 5–joint 6	0.089
joint 6–joint 7	0.106
joint 7–joint 8	0.084
joint 8–joint 9	0.072
joint 9–joint 10	0.076
joint 10–joint 11	0.093
joint 11–tail	0.066
tail fin	0.320
forelimb upper leg	0.143
forelimb lower leg	0.100
hindlimb upper leg	0.118
hindlimb lower leg	0.100
ball foot radius	0.015

than water, which is important in order for the robot to be able to be sufficiently submerged in water. The ball-shaped feet are made out of silicone rubber moulded around a three-dimensionally printed spherical structure attached to steel rods that act as the lower leg of each limb. The robot dimensions and specifications are summarized in table 2 and electronic supplementary material, table S1.

In the swimming experiments, the robot, including the passive tail fin, was entirely covered by means of two protective suits (figure 3*d*). The outer suit was made of a Lycra® Nylon fabric laminated with a 1 mm layer of polyurethane (PU) that ensures waterproofness. Seams were sealed by taping the same fabric from the inside (PU–PU connection). A waterproof zipper (TIZIP, MasterSeal 10, 500 mbar pressure proof) was used to open and close the suit. The purpose of the inner suit (made of soft fabric) was to protect the sensitive PU layer from sharp edges on the robot. In order to allow limb interaction with the environment in water, the feet had to be kept outside the suit. Therefore, the steel rods at the crus/antebrachium were guided through a cylindrical silicone rubber piece that was glued inside the suit at each of the limbs. The press fit between silicone and the rod ensures waterproofness. To provide power to the robot, we used IP67, binder 693 series, four-pole plug/socket connectors, as part of a 5 m tether (there is also the option to have a tetherless set-up with a battery pack).

The swimming suit notably increases the volume of the robot, which increases the buoyancy. Therefore, the robot is not fully submerged in water. On the positive side, this adds a stabilizing property (no rolling); however, we noted that lateral movement of the body was increased substantially, especially in the rostral part. Consequently, for the experiments, we added a weight of 1.5 kg at the head as well as 1 kg at the level of the hind girdle. Furthermore, the air inside the suit was vacuumed to decrease the overall volume as much as possible.

2.4. Transformation to joint angles for Pleurobot

Finally, given the introduced design methodology, it is possible to impose kinematics recorded from the animal on Pleurobot. We will show in §5 how this together with a careful scaling analysis (§4) can be used to validate our design. To transfer the cineradiographic movement recordings to Pleurobot, we solve two optimization problems related to the spinal and limb joints, respectively. Note that in this optimization problem as opposed to that for the robot design, the segment lengths are given, and we solve for the joint angles. Motion sequences from the three-dimensional reconstruction of the cineradiographic recordings contained between 12 and 190 timesteps.

To compute the corresponding spinal joint angles for Pleurobot, the trunk and tail postures of *P. waltl* were first approximated using piecewise linear segments, where the length of each segment was given from the spinal segmentation on Pleurobot. Subsequently, at each time instance, within a particular movement cycle (with 40 fps for swimming and 80 fps for walking), we solved an optimization problem as follows

$$\{x_{i+1}, y_{i+1}\} = \min_{x_{i+1}, y_{i+1}} \left(\int_{x_i}^{x_i+1} \left| y_t(x) - \left(y_i + \frac{y_{i+1} - y_i}{x_{i+1} - x_i}(x - x_i) \right) \right| \mathrm{d}x \right) \tag{2.1}$$

In this planar problem, $y_t(x)$ describes the target posture in Cartesian coordinates. x_i and y_i denote coordinate points corresponding to the ith joint on Pleurobot. As shown in equation (2.1), the optimization problems are solved sequentially, starting from the first (head) until the last joint (tail). The problem was solved using the unconstrained nonlinear optimization function fminsearch from Matlab, with default parameters. The solutions provide us with a piecewise linear approximation of the posture $y_t(x)$. Finally, the joint angles can be extracted by computing the relative angles between segments.

Related to the limb joint angles, the postures on *P. waltl* were identified by means of five tracking points located at the hip, the femur–crus joint, the crus–tarsus joint, the metatarsus–phalanges joint and the mid-phalanx tip (and corresponding points in the forelegs). The postures (again at each time instance) had to be approximated by the segmented robot limbs, where the first segment represents femur/humerus and the second segment the connection from elbow/knee to the metatarsus. In order to compute the corresponding yaw, pitch, roll and elbow/knee angle, we set up an inverse kinematics optimization problem for each posture:

$$\underline{\varphi} = \min_{\underline{\varphi}} (|p_{d1} - p_1(\underline{\varphi})| + |p_{d2} - p_2(\underline{\varphi})|), \tag{2.2}$$

where $\underline{\varphi}$ describes the joint angles, p_{d1} and p_{d2} indicate the three-dimensional positions of shoulder/hip and elbow/knee joints on *P. waltl* and the corresponding forward kinematics on Pleurobot are described by $p_1(\underline{\varphi})$ and $p_2(\underline{\varphi})$.

3. Dynamical scaling

Ideally, our robot should have a similar size to its biological counterpart. However, owing to the unavailability of powerful miniature actuators at this stage in technology and our particular choice of servomotors, we are dealing with a robot that

is geometrically scaled up by a factor of 8.6 with respect to *P. waltl*. Similar to other studies [9,45,46], it was therefore important to perform a dynamical scaling study, so that the robot could faithfully be used to investigate locomotion of the salamander, in aquatic and terrestrial environments. This is necessary to ensure that the physical interactions with the environment are dynamically equivalent, for instance in terms of hydrodynamics regimes.

In this context, an important question was how the robot should apply movements at speeds and while exerting forces that are comparable to the salamander. Based on the proposed design methodology, relative lengths of different body elements (geometric scaling) as well as the range of joint angles remained the same as for *P. waltl* (except for a 1.67 times increased robot head size, owing to the placement of the control board). As a consequence, it was also ensured that the robot operates in the same range of movement. To incorporate the speeds and forces, we also used the criterion for dynamic similarity as defined by Alexander [47]

$$\frac{mv^2}{Fl} = \text{const.} \tag{3.1}$$

where m denotes the total body mass, v is the forward moving speed and l is the characteristic length of the robot. F describes the main forces that act on the system while moving. Dynamic similarity has been used to compare different types of gaits across animals as well as to analyse, for instance, the relation of mass and locomotion speed in animals of different sizes [48–50]. Let g, ρ, μ, f be the gravitational acceleration, fluid density, dynamic viscosity and the frequency, respectively, then the Froude $\left(Fr = v/\sqrt{gl}\right)$, Reynolds $(Re = \rho l v/\mu)$ and Strouhal $(St = fl/v)$ numbers are non-dimensional quantities that can be obtained from the dynamic similarity criterion (equation (3.1)). The Froude number is typically used to compare walking gaits, where gravitational forces are dominant [6].

By definition the Reynolds number determines the type of interaction forces with mainly viscous forces at low *Re* numbers and inertial forces at high *Re* numbers. The *Re* number was measured between 1.45×10^4 and 7.81×10^4 in the experiments with *P. waltl* and between 1.97×10^5 and 4.48×10^5 in our swimming experiments for Pleurobot. These high numbers indicate that both animal and robot are in a regime where inertial forces have a greater influence compared with viscous forces. Furthermore, it is important to note that in the particular case of *P. waltl* (as well as Pleurobot) we are analysing swimming at the water surface. Surface swimming is defined as swimming at a depth that is smaller than one body length [51,52]. It is considered a special case as 'drag is increased substantially owing to the formation of waves' [53] and the wave resistance force is a function of the *Fr* number [54]. Therefore, we can expect to have dynamically similar behaviour at similar *Fr* numbers, which is also supported by common practice in naval architecture [55], where the *Fr* number is used to create dynamically similar models of ships. Finally, related to periodic movements, the *St* number can be used to analyse movements at different frequencies. Intuitively, this measure covers observations in which smaller animals generally tend to move at much higher frequencies than bigger animals [56].

Based on the *Fr* and *St* numbers, which should be the same for the robot and the animal, we use the subsequent scaling law to determine the corresponding speeds and locomotion frequencies on the robot in order to conserve dynamic similarity with *P. waltl*

$$v_{\text{robot}} = \sqrt{\frac{l_{\text{robot}}}{l_{\text{salamander}}}}\, v_{\text{salamander}} \tag{3.2}$$

and

$$f_{\text{robot}} = \sqrt{\frac{l_{\text{salamander}}}{l_{\text{robot}}}}\, f_{\text{salamander}} \tag{3.3}$$

Accordingly, given that the ratio $l_{\text{robot}}/l_{\text{salamander}}$ is 8.6, we should be able to obtain dynamically similar behaviour by scaling the salamander speeds by 2.94 and frequencies by 0.34 for walking and swimming.

4. Experimental validation of Pleurobot

To verify the design of our robot and to quantify the locomotor abilities with respect to *P. waltl*, we carried out a series of experiments and compared kinematics as well as dynamics. For this, we replicated walking, swimming and aquatic stepping gaits by replaying the precise body posture sequences that were obtained from cineradiographic recordings. Of course, by design, Pleurobot is made to incorporate all the necessary DOFs in order to replay fairly closely the joint kinematics for the three recorded gaits. But rather than focusing on the joint kinematics themselves, we ask the question of how the robot locomotes using those (i.e. how it progresses from one place to another and, more generally, how its orientation changes in three-dimensional space).

The aims of the following experiments are (i) to demonstrate that we can reproduce the two basic behaviours of the salamander, so well that it has the potential to reproduce more complex locomotor behaviours if these are recorded from the animal and (ii) to validate whether replaying kinematics recorded from the animal, provided the scaling factors, can yield behaviours (i.e. Cartesian kinematics and ground reaction forces, GRF) comparable to the salamander's. Especially the second point will help us validate future experiments in which Pleurobot is driven by a neuronal model instead of pre-recorded animal kinematics.

4.1. Experimental set-up for robot experiments

In order to capture the movements for the walking experiments of the robot, we collected the motion capture data (MOCAP). A total of 14 MOCAP cameras (Optitrack s250e, Naturalpoint, Inc. 2011) together with 13 infrared reflective markers (11 mm) were used for this purpose. The markers were positioned at the each of the spinal joints (10 markers), additionally a rigid body marker (three markers) was fixed on the head. Movements were recorded at 240 frames per second. Marker trajectories were processed in Arena (Naturalpoint, Inc. 2011) and Matlab (Matlab 2014b, MathWorks, Inc.). We conducted five experiments for frequencies of 0.1, 0.2, 0.3, 0.4, 0.5 Hz, where each experiment included six trials which were all part of the overall gait analysis.

The swimming experiments were carried out in a pool with dimensions 6 m × 1.5 m with a water level of 18–22 cm. Movements were recorded with a camera (Canon PowerShot S120), which was mounted at a height of 2 m over the pool at a frame rate of 30 frames per second and a resolution of 1920 × 1080. In addition, we used a video-tracking system as

described in [57] to track an LED mounted on the robot. During the swimming experiments with the robot, the limbs were folded against the body. The forelimbs were folded underneath the body by positioning the humerus pointing backwards and parallel to the trunk, and fully flexing the elbow joint (as opposed to *P. waltl* which extends the elbow joint). The hindlimbs were also folded underneath the body in a way that is qualitatively similar to *P. waltl*, where the femur was positioned pointing backwards at about an angle of 45° with respect to the trunk. The crus was extended at about 135° (45° from full extension). We chose not to use the original limb trajectories during swimming as in *P. waltl* for two reasons. First, constraints from the suit did not allow us to exactly reproduce the limb kinematics in swimming, as the tension caused by the stretched material would have restricted the undulatory movements along the trunk. Second, using a fixed limb posture made the experiments more repeatable (same drag coefficient for same body shape) and allowed us to investigate and compare the movements along the spinal joints under same conditions for different swimming gaits. In any case, the limb movements of *P. waltl* during swimming are minimal. For the swimming experiments, we considered two different animal gaits, which were tested at four different frequencies. To show the repeatability of the experiments, three trials each were performed.

4.2. Characterization of locomotion

To compare the movements between Pleurobot and *P. waltl*, we investigated their lateral displacements and forward velocities. These quantities were measured with reference to the line of locomotion that was computed with the following linear regression

$$\{m_k, q_k\} = \min_{m_k, q_k} \left(\sum_{i \in P_k} |y_i - m_k x_i - q_k|^2 \right), \qquad (4.1)$$

where k denotes the kth cycle and m_k, q_k are the resulting slope and offset of the regression. P_k describes the set of all tracked spinal points with coordinates (x_i, y_i) in the kth cycle. The robot lateral displacement for walking was computed based on the MOCAP recordings and from video data for the swimming gaits. In the case of swimming, characteristic midline points were computed in two steps. First, a curve was fitted (spline interpolation) through 21 manually selected points along the hypothetical midline of the body. The starting point of the midline was defined as the tip of the head and the endpoint was defined as the end of the tail. The midline was then resampled to 13 equidistant points. For *P. waltl*, the corresponding measure was computed based on the cineradiographic tracking data.

Forward velocity of the robot was computed in steady state, which was reached starting from the second locomotion cycle for walking and starting from the third locomotion cycle for swimming. The corresponding forward displacement over time was then averaged over two cycles for walking and three cycles for swimming. The rigid body marker and the LED marker were used as reference markers, respectively.

Besides the above-mentioned kinematic measures, we furthermore recorded GRFs on the robot for part of the validation. In this context, forces in three dimensions were recorded using force plates (type 9260AA3, Kistler, 2011) at a sampling frequency of 1 kHz. The GRFs were measured for both front and hindlimbs. To select appropriate experimental runs for the analysis, video recordings were obtained during the measurements. Only experiments in which the robot was walking straight and only a single foot was touching a force plate were taken into account. Finally, seven experimental runs for the front limbs and eight experimental runs for the hindlimbs were selected for the analysis. The data were processed using Matlab (Matlab 2014). The stance phases within a cycle were extracted, using the normal force profile for the front limbs (force indicating stance, no force indicating swing). For the hindlimbs, as a matter of fact, in many experiments, the foot was slightly touching the ground when protracting. Therefore, the stance phase for the hindlimbs was identified, using the anteroposterior as well as the normal force profile. As such, the beginning of stance was identified as soon as propulsive force (retraction) was registered, whereas the end of stance (lift off) was defined when the normal force dropped to zero. This is consistent with the force measurements in [58], where propulsive stance was also analysed. Furthermore, forces were smoothed using a moving average filter ($n = 100$, over/under smoothing was checked visually). For the analysis, the stance duration was normalized from 0% to 100% in order to compare the different experiments. All the forces were expressed with respect to the percentage of body weight, which facilitates the comparison with the salamander.

4.3. Walking

During ground locomotion, *P. waltl* typically uses two types of gaits, the walking trot and the lateral sequence walk [36,43]. Both gaits involve trunk and tail movements that oscillate with an S-shaped standing wave. When well coordinated with the limbs, this allows the animal to maximize its stride length. As part of the validation, we replicated an example lateral sequence walking gait on Pleurobot and discovered interesting similarities (figure 4).

Based on the scaling laws introduced in §4, it can be shown that the stride length, which is defined as the forward speed normalized by the product of frequency and characteristic length, is a necessary quantity to be matched in order for two motions to be dynamically similar. The resulting stride lengths were measured in the range of 0.55–0.74 SVL of several repeated experiments at different frequencies on the robot (figure 5) and from 0.7 to 0.84 SVL for *P. waltl*. In this range, we achieve the best matches at 0.2 Hz (7.8% error) and 0.3 Hz (3% error) with respect to the animal's gait, which corresponds to a frequency of 0.19 Hz when dynamically scaled. The lower stride lengths can be expected and are in accordance with the abstraction of the ball-shaped feet, as propulsive power from the phalanges is not included. In addition to forward movement, we also analysed the lateral displacement patterns (inset in figure 5) as a means to quantify characteristics perpendicular to the movement direction.

We found that the profile with the local minima at the two girdles could be reproduced indicating that the trunk oscillations comply with *P. waltl*. The smaller lateral displacement in the trunk is a result of the slightly different oscillation pattern along the line of locomotion, where the rostral part of the robot tends to oscillate more than that of the salamander (figure 4, lateral movement of the neck joint). Therefore, the lateral oscillation span of the trunk along the line of locomotion is reduced.

To quantify further similarities between the Pleurobot and *P. waltl*, we compared the footfall patterns. For this purpose,

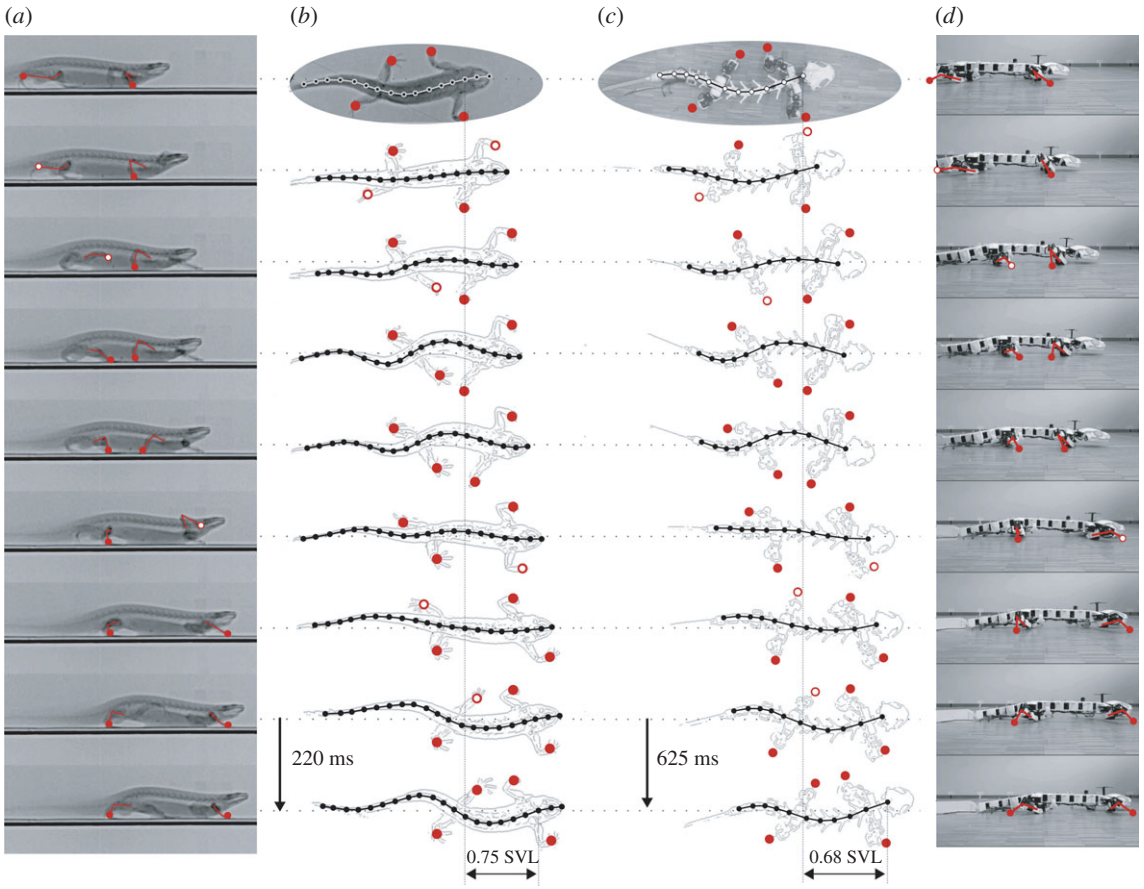

Figure 4. Comparison of walking gaits from *P. waltl* and Pleurobot. The left-hand side shows side view (*a*) and top view (*b*) of a *P. waltl* walking gait cycle at 0.57 Hz, obtained from cineradiographic recordings. The red filled circles indicate stance phase and the white filled circles indicate swing. The right-hand side shows top view (*c*) and side view (*d*) of Pleurobot replaying the corresponding *P. waltl* gait at 0.2 Hz, respecting dynamic scaling. The fine dashed lines in the top views indicate the line of locomotion, computed as linear regression of all the midline points within the gait cycle. Stride lengths are indicated by means of snout–vent length (SVL).

the absolute contact force at each individual foot was measured using force sensors (Optoforce, OMD-D30 3D Force Sensor). A threshold of 7 N (10% body weight) was used to discriminate between stance and swing. At the same time, the limb kinematics were recorded via the joint encoders of the servomotors, which provided joint angle measurements at a sampling time of 12 ms with a resolution of 0.088°. As shown in figure 6, the forelimb footfalls can be accurately reproduced on the robot, showing very similar stance and swing durations as well as timings (electronic supplementary material, §2). The hindlimbs of the robot show shorter stance durations than *P. waltl* (left hind: robot $53.38 \pm 0.99\%$ (mean $\pm$ s.d.), *P. waltl* $78.64 \pm 5.08\%$, $p = 2.84 \times 10^{-7}$, $\mu_{\text{robot}} > \mu_{\text{animal}}{}^2$; right hind: robot $64.30 \pm 0.47\%$, *P. waltl* $80.06 \pm 4.29\%$, $p = 9.40 \times 10^{-8}$, $\mu_{\text{robot}} > \mu_{\text{animal}}$), which is expected because of the following reasons: the ball-shaped foot on Pleurobot represents the corresponding metatarsus in the animal and the phalanges are therefore not modelled on the robot. This is especially notable in the hindlimbs, which have longer phalanges. As a result, the hindlimbs on the robot show systematically shorter stance durations, despite similar touch-down timings.

4.4. Swimming

Owing to its amphibious nature, *P. waltl* can not only exploit gaits in terrestrial, but also in aquatic environments. Two major steady-state gaits can be observed: swimming and aquatic stepping. The latter is predominantly used when the animal is able to reach the aquatic ground with its limbs. It resembles a trotting pattern in which short power strokes of the diagonal limb pairs in coordination with spinal undulations lead to forward propulsion. Additional analysis of this gait is presented in the electronic supplementary material. Here, we focus on swimming and ask whether we can replay gaits in the same way as we do for walking.

Pleurodeles waltl swims using an anguilliform swimming gait in which a travelling wave of body undulation is propagated from head to tail [10] (figure 7, left). The outcome in terms of forward propulsion for replayed salamander swimming gaits on the robot is more difficult to predict than for walking, as the dominant interaction forces (drag) are hard to estimate for a body with such a complex geometry. Nevertheless, the animal swimming gaits could be reproduced on the Pleurobot as shown in figure 7, demonstrating similar forward progression and overall attitude between animal and robot along the line of locomotion. *P. waltl* showed a great variety of stride lengths across different recorded gaits ranging from 0.17 body length (BL) up to 0.5 BL. Similar to the Axolotl (*Ambystoma mexicanum*), also an anguilliform swimmer, these stride lengths are achieved not only by changing the frequency, but also by changing the amplitude profile along the body [58]. In our experiments, we observed, for example, significantly increased tail amplitudes in gaits with a higher resulting stride length.

When replicating swimming gaits with large amplitudes and high frequencies, we observed large tracking errors

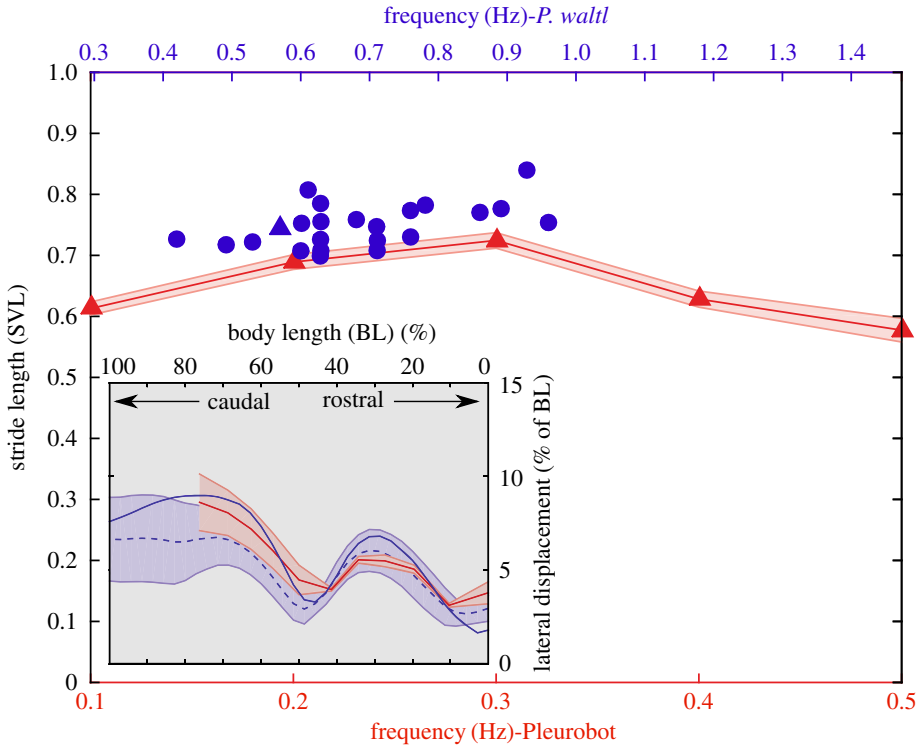

Figure 5. Similarities in stride length and lateral displacement for walking. Stride length for walking was defined as forward speed divided by frequency normalized by snout–vent length. Data from *P. waltl* in blue and from Pleurobot are indicated in red. The Pleurobot data are represented as mean and standard deviation of six runs at frequencies 0.1, 0.2, 0.3, 0.4, 0.5 Hz. The frequencies of observed gaits from *P. waltl* are scaled based on the scaling laws for dynamic similarity with a factor of 0.34. The blue triangle represents the particular gait that was replayed on Pleurobot, blue discs represent other gaits from *P. waltl*. Inset: lateral displacement for terrestrial stepping computed by means of maximal displacement from the line of locomotion. The blue-shaded area shows mean (dashed line) and standard deviation of 23 cycles obtained from *P. waltl*. The blue solid line represents the particular *P. waltl* gait that was replayed. The red-shaded area shows mean and standard deviation from six runs of the particular gait replayed on Pleurobot at 0.2 Hz.

(electronic supplementary material). This is related to the torque and speed limits of the motors, which result in a limited control bandwidth. Therefore, we focused our analysis on gaits with smaller stride lengths. Subsequently, the reproduced gaits (figure 8) resulted in a similar range of stride lengths to those of the salamander (robot: 0.21 ± 0.05 BL (mean $\pm$ s.d.); salamander: 0.22 ± 0.04BL; $p = 0.55$, $\mu_{\text{robot}} = \mu_{\text{salam}}$).

Note that the decrease of stride length with frequency in the robot is likely owing to an increase of tracking errors that prevent the exact replication of the gaits at higher frequencies (see electronic supplementary material, figure S1). This explains why the stride lengths are smaller in the robot at frequencies of 1.18 and 1.28 Hz (blue square and triangle in figure 8) that would be required for both animal gaits based on the scaling analysis.

We were able to obtain a very similar lateral displacement profile (inset in figure 8, electronic supplementary material, figures S5 and S6) showing increasing values from head to tail. Indicating that on the robot, as on its biological counterpart, the lateral movement of the rostral part is kept minimal.

4.5. Ground reaction forces: comparison between salamanders and Pleurobot

We finally asked how the interaction forces between the robot and the environment along with the kinematics relate to *P. waltl* and quantified them by measuring GRFs for a walking gait. Based on the scaling law for speed, equation (2.1) (dynamic similarity) reduces to the ratio of body weight and the experienced external force. Therefore, we can expect dynamic similarity between Pleurobot and *P. waltl* when the external forces (GRFs) normalized by the body weight are similar.

GRF measurements obtained for Pleurobot were compared with data from Kawano & Blob [59] reported for *Ambystoma tigrinum*, because measurements were not available for *P. waltl*. Compared with *P. waltl* (mean stride length: 0.75 SVL), similar stride lengths were observed for the *Ambystoma tigrinum* (mean stride length: 0.68 SVL for forelimbs, 0.73 SVL for hindlimbs, SVL: 0.1 m, BL: 0.187 m, [59]). The results of the GRF analysis are presented in figure 9, where the salamander shows characteristic normal peak forces at 60.2% stance for the front limbs and at 24.7% of the stance phase for the hindlimbs. It indicates that the front limbs are making a significant effort to push the body weight off the ground in the second half of the stance, whereas the hindlimbs have to bear most of the vertical load in the beginning of the stance phase. Experiments of walking with the robot showed qualitatively similar normal force profiles, where normal forces peaked at ($61.2 \pm 1.3\%$ (mean $\pm$ s.d.), $p = 0.1$, $\mu_{\text{robot}} = \mu_{\text{animal}}$) for forelimbs and ($27.3 \pm 1.5\%$, $p = 0.002$, $\mu_{\text{robot}} = \mu_{\text{animal}}^3$) for hindlimbs. Furthermore, *Ambystoma tigrinum* systematically showed GRFs in medial direction (front: $-0.047 \pm 0.011\%$ BW (mean $\pm$ s.d.), $p = 1$, $\mu < 0$; hind: $-0.042 \pm 0.02\%$ BW, $p = 1$, $\mu < 0$; i.e. external forces with respect to the salamander point medially for both forelimbs and hindlimbs), suggesting that the salamander pushes its legs laterally from the body during stance. These characteristics are partially reproduced by the forelimbs of the robot, which on average also produce a positive lateral push ($-0.035 \pm 0.043\%$ BW), but not for the hindlimbs ($-0.003 \pm 0.025\%$ BW) where a mostly neutral trend is observed.

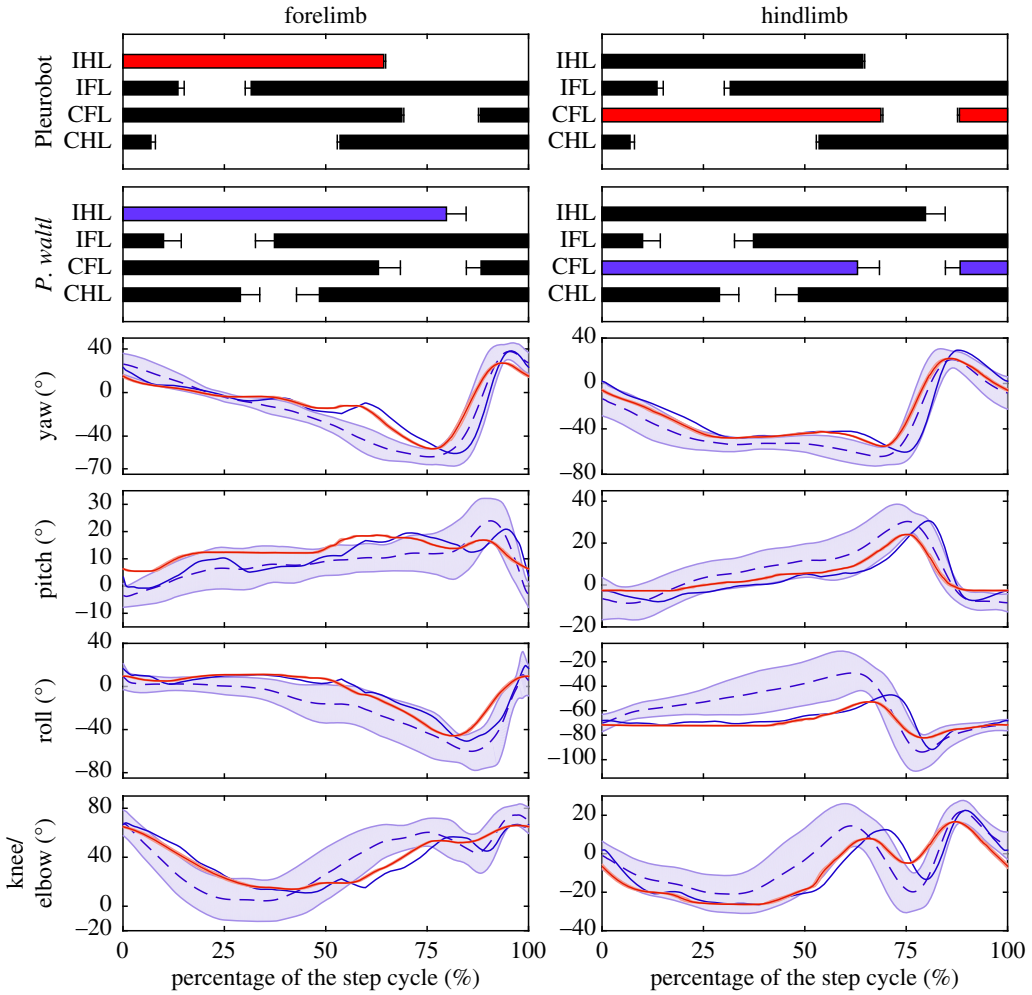

Figure 6. Similarities in limb kinematics and footfall patterns for walking. The top two panel rows represent Hildebrand diagrams show stance (black) and swing (white) phases within a normalized gait cycle. IHL, ipsilateral hindlimb; IFL , ipsilateral forelimb; CFL , contralateral forelimb; CHL, contralateral hindlimb. The left-hand side shows results for the hindlimbs and the right-hand side for forelimbs. In the other panels, blue-shaded areas represent mean and standard deviation of joint angle trajectories for *P. waltl* (23 cycles), blue solid lines indicates a particular salamander gait. Red-shaded areas indicate mean (solid line) and standard deviation of the particular replayed gait on Pleurobot (five gait cycles at 0.2 Hz, based on a scaling factor of 0.34 respecting dynamic similarity).

Finally, Kawano & Blob's data [59] show that most of the propulsion in the salamander is generated by its hindlimbs indicated by the anteroposterior forces, which are close to zero ($-0.011 \pm 0.015\%$ BW) for the front limbs and systematically positive (propulsive) for the hindlimbs ($0.097 \pm 0.042\%$ BW, $p = 1$, $\mu > 0$). We could find the same characteristics for the corresponding robot gait (front: $-0.007 \pm 0.040\%$ BW; hind: $0.077 \pm 0.058\%$ BW, $p = 1$, $\mu > 0$), although showing larger fluctuations in force magnitude in the front limbs.

5. Discussion

We presented a possible way of designing biorobots in a systematic way and outlined the design procedure, which is based on high-speed cineradiographic recordings and numerical optimization, along with kinematic and dynamic validation respecting physics scaling laws. We used the approach to construct Pleurobot, a salamander-like robot with 27 DOFs that can emulate the walking and swimming gaits of the salamander *P. waltl*.

It could be seen as trivial that Pleurobot's locomotion matches that of the real salamander, because the robot replays the sequence of animal postures. Moving a robot with predefined joint angle trajectories is indeed trivial in the sense that it will, given a good controller and strong actuators, produce the expected robot postures. However, unlike automatons in amusement parks that are solidly fixed to the ground, Pleurobot's displacements in three-dimensional space are the results of (complex) physical interactions between the internal movements of the robot and the environment. The robot must be properly designed such that the interaction forces match those of the animal [60]. For instance, during ground locomotion, inaccurate mass distribution could lead to incorrect body orientations and incorrect contact with the ground (e.g. a limb not touching the ground when it should) and hence different locomotor patterns and locomotion speeds. Similarly, the swimming of the robot could be very different from that of the animal if geometrical and dynamical properties of the robot had not been properly adjusted with the dynamic scaling. The indirect (stride lengths and lateral displacements) and direct (GRFs) comparisons between robot and animal presented here indicate that the interaction dynamics closely correspond.

Our approach results in a physical tool that provides an interface between computational models and the environment on which rich motor skills can be tested in the future. The success of our approach is of course tested with behaviours with slow dynamics like those typically seen in salamanders and in particular *P. waltl*. In principle, it could be applied to the

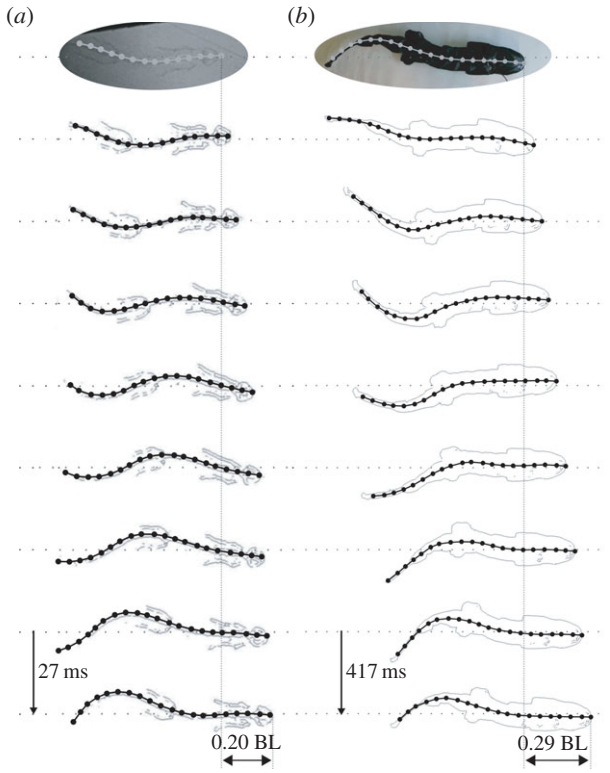

Figure 7. Comparison of swimming gaits from *P. waltl* and Pleurobot. Panel (*a*) shows a *P. waltl* swimming gait cycle at 3.8 Hz from top to bottom divided in nine snapshots. Panel (*b*) shows the same gait replayed on Pleurobot at 0.3 Hz. The bold dotted line indicates the midline of robot and animal. The horizontal fine dotted lines indicate the line of locomotion, computed with a linear regression of all the midline points within a gait cycle.

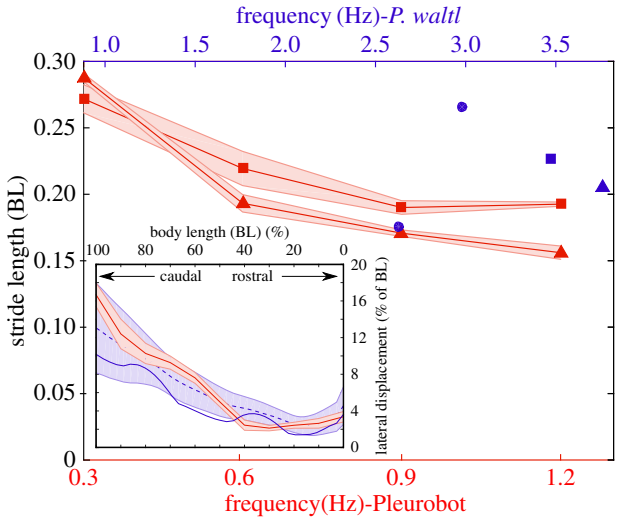

Figure 8. Similarities in stride length and lateral displacement for swimming. Stride length for swimming was defined as forward speed divided by the frequency and normalized the body length. Data from *P. waltl* are shown in blue and from Pleurobot in red. The Pleurobot data are represented as mean and standard deviation of three runs each at frequencies 0.3, 0.6, 0.9, 1.2 Hz. The observed gait frequencies from *P. waltl* are scaled based on the scaling laws with a factor of 0.34. The blue triangle and square represent the particular gaits that were replayed on Pleurobot represented as red triangles and squares, respectively. The blue circles show two additional trials from *P. waltl*. Inset: lateral displacement for swimming computed by means of maximal displacement from the line of locomotion. The blue-shaded area shows mean (dashed line) and standard deviation of 20 cycles obtained from *P. waltl*. The blue solid line represents a particular *P. waltl* gait that was replayed. The red-shaded area is showing mean and standard deviation from 10 runs of the particular gait replayed on Pleurobot at 0.3 Hz.

design of other types of robots that match different animals and modes of locomotion provided that the model is able to capture the dynamic conditions. Cineradiography allows one to observe bone movements, from which detailed and accurate kinematic information can be extracted. This allows one to identify locomotion-relevant joints (active or passive). Compared with motion capture based on markers and cameras, it prevents possible problems of movements of surface markers owing to motion of soft tissues [61], and of occlusions. It has however the disadvantages that more work is required to extract the three-dimensional data frame by frame from the biplanar images (either manually, like in our case, or through machine vision algorithms), and that the recording volume is limited.

In our case with *P. waltl*, optimization based on kinematic data was then sufficient to find a good robot design. We were able to replay gaits on the robot without modulating gaits based on feedback. For other animals and other modes of locomotion, similar steps could be taken but additional mechanical design and control steps could be necessary. For instance, it might be needed to use remote actuation with cables in order to obtain the right mass distribution as for the cat-like robot Cheetah-Cub [62]. Different gaits on other robots might also need explicit feedback control (e.g. for balance), whereas we are benefiting from the intrinsically stable sprawling posture of the salamander. The choice of servomotors was convenient in our design of a salamander-like robot. It substantially decreases the time and cost to build and transform. However, more generally, other actuators (e.g. with low gear ratio, passive elements, etc.) could be used depending on the type of locomotion and the questions that have to be addressed.

We furthermore applied the scaling laws that have to be respected in order to obtain dynamic similarity between the robot and the animal. For the salamander, it was shown that the Froude number had to be used for walking and surface swimming. In other cases, such as e.g. deeper three-dimensional swimming (depth larger than a body length), the Reynolds number should be used.

The analysis of footfall patterns and the aquatic stepping experiments (electronic supplementary material) revealed the limitations in the current design of Pleurobot with respect to its biological counterpart *P. waltl*, indicating that the role of the phalanges is important for stepping locomotion (in terrestrial and aquatic environments). The abstraction of the feet to single contact points is an important simplification that makes Pleurobot less of an anchor than the original aim. However, future versions will focus on integrating as many aspects of the foot as possible given their complexity. Furthermore, actuator limitations in size and power currently restrict the reproduction of some dynamically similar swimming motion, especially at higher frequencies and stride lengths. However, our approach shows promising results for the reproduction of walking patterns of the salamander *P. waltl* that conserve respective characteristics such as stride length, footfall patterns as well as similar GRFs.

One aspect that we did not address is internal dynamics [63], i.e. how internal forces and torques generate body deformations (i.e. postures). In the animal, body deformations are due to sets of muscles acting on the joints, whereas in the robot, they are due to torques produced by the PD controllers of the servomotors. There are some similarities between the

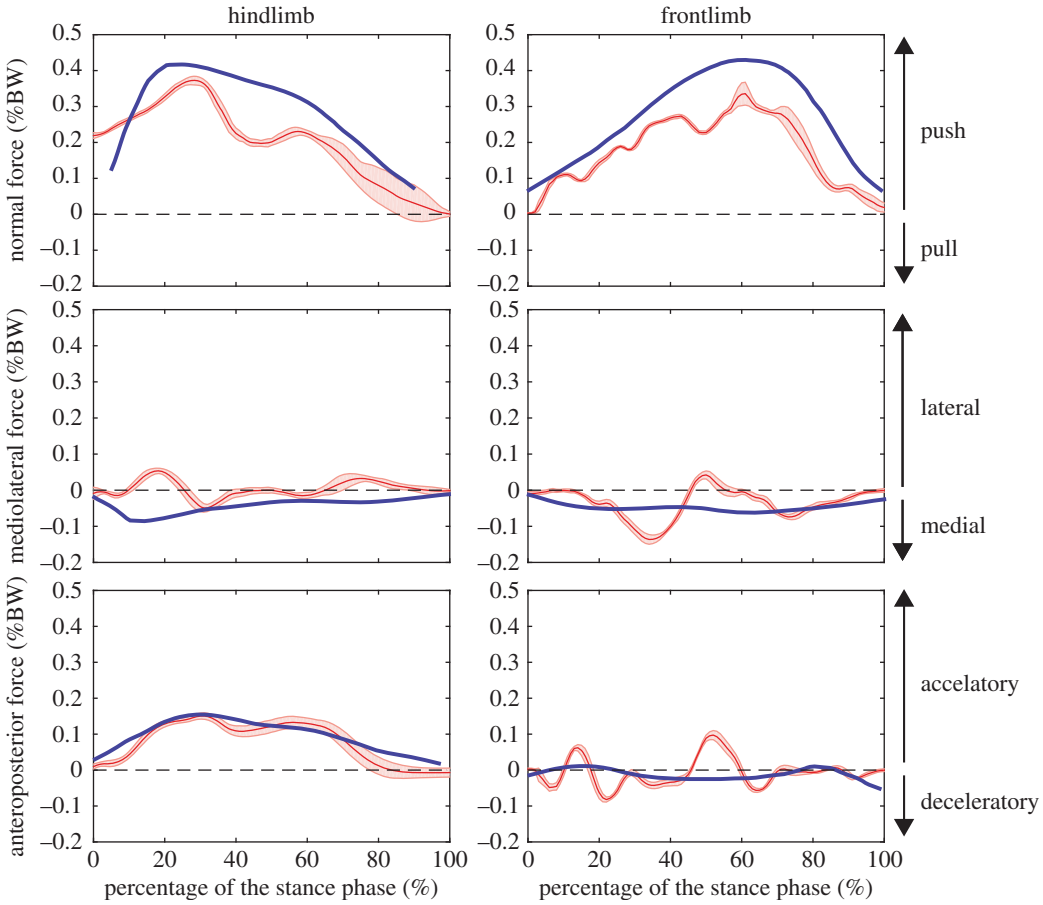

Figure 9. Comparison of ground reaction forces (GRFs) in the *Ambystoma tigrinum* and Pleurobot. Hind (left side) and front (right side) limb GRFs were measured and analysed with respect to normal, sideways and forward contribution. Red-shaded areas represent Pleurobot experiments (seven cycles for forelimbs and eight cycles for hindlimbs) with mean and standard deviation. The blue solid lines indicate mean data from the *Ambystoma tigrinum* [58]. The forces were normalized by means of body weight and only propulsive stance was considered for the analysis. The dashed line indicates zero forces.

two types of actuation, because with the proportional P and derivative D gains elasticity and damping can be adjusted to some extent. Nonetheless, there are also important differences: (i) antagonist muscles allow the change of stiffness and (ii) multiarticular muscles act on more than one joint. Muscle properties can be simulated if the gearboxes are back-drivable (or torque sensors with very fast control loops are available) and when the motors are used to control direct torque output. Given motors with these properties, this will allow us in the future to investigate the role of muscle properties in locomotion and to address questions related to locomotion efficiency (for instance how to obtain a given speed with minimal muscle activation, i.e. minimal metabolic cost). There is also the possibility to add elastic elements in series [62,64,65] to provide mechanical elasticity and energy restoration.

In the future, we envision Pleurobot as a useful tool for neuroscience. Locomotion is the result of interaction of many components, and a physical model such as Pleurobot can provide the interface between, on the one hand, computational models of the nervous system and of muscles, and, on the other hand, physical interactions with terrestrial and aquatic environments. As a realistic physical model of the salamander capable of emulating basic and complex behaviours, it can serve to test hypotheses about the interactions between the different components underlying locomotion, in particular the interactions between descending modulation, central pattern generation, sensory inputs and interaction forces from the environment. Compared with our previous robots and previous studies, the robot will for instance allow us to investigate (i) the organization of the limb CPGs with multiple neuronal oscillators (similarly to what has been found in the salamander [66]), (ii) the effect of adding more descending pathways to our spinal cord models, and (iii) the generation of a larger variety of motor behaviours such as turning, walking backwards, scratching, paddling, etc.

Obviously, it is by performing these future studies that we will really validate the design methodology presented in this article and its usefulness for neuroscience. It is possible that additional design iterations might be needed (for instance with the addition of more DOFs, the replacement of motors with stronger ones, the use of cables for remote actuation, the addition of sensors, etc.), but the current robot already opens the door to many investigations.

Furthermore, other fields, including functional morphology, palaeontology and field robotics, might benefit from the robot or its design methodology. In terms of robotics, an amphibious salamander-like robot capable of locomotion in different environments could find useful applications for inspection or search-and-rescue operations.

Authors' contributions. K.K. developed the design methodology, evaluated cineradiographic data, designed and built the robot, programmed the robot, and designed robot experiments; R.T. evaluated cineradiographic data, designed and evaluated robot experiments, and contributed to the final manuscript; K.M. designed and evaluated robot experiments, introduced the scaling methodology, and contributed to the final manuscript; T.H. helped with robot experiments and programmed the robot; N.K.M. evaluated cineradiographic data; S.T. contributed to the scaling methodology; J.M.C. contributed to collect cineradiographic data and helped with

the final manuscript, A.J.I. directed the project and contributed to the design methodology and to the final manuscript.

Competing interests. We declare we have no competing interests.

Funding. We acknowledge financial support from the Swiss National Center of Competence in Research in Robotics, and from the Swiss National Science Foundation (project CR23I2_140714).

Acknowledgements. We are grateful to Dr Martin Fischer at the University of Jena, Germany, for providing access to the cineradiography equipment and to Dr Nadja Schilling for helping with the experiments.

Endnotes

[1]A type of evolutionary optimization algorithm that evolves a population of candidate solutions by altering and mutating them with the goal to maximize a selected fitness criterion.

[2]We carried out standard t-tests with $\alpha = 0.05$ throughout this study, $\mu_i > \mu_k$ indicates the null-hypothesis. $p < 0.05$ indicates that the null-hypothesis should be rejected.

[3]Notice that the values differ statistically, however there is a qualitative similarity.

References

1. Dickinson MH, Farley CT, Full RJ, Koehl MAR, Kram R, Lehman S. 2000 How animals move: an integrative view. *Science* **288**, 100–106. (doi:10.1126/science.288.5463.100)
2. Daley MA, Biewener AA. 2006 Running over rough terrain reveals limb control for intrinsic stability. *Proc. Natl Acad. Sci. USA* **103**, 15 681–15 686. (doi:10.1073/pnas.0601473103)
3. Engberg I, Lundberg A. 1969 An electromyographic analysis of muscular activity in the hindlimb of the cat during unrestrained locomotion. *Acta Physiol. Scand.* **75**, 614–630. (doi:10.1111/j.1748-1716.1969.tb04415.x)
4. Grillner S, Degliana T, Ekeberg Ö, El Manira A, Lansner A, Orlovsky GN, Wallén P. 1995 Neural networks that co-ordinate locomotion and body orientation in lamprey. *Trends Neurosci.* **18**, 270–279. (doi:10.1016/0166-2236(95)80008-P)
5. Cabelguen J-M, Bourcier-Lucas C, Dubuc R. 2003 Bimodal locomotion elicited by electrical stimulation of the midbrain in the salamander *Notophthalmus viridescens*. *J. Neurosci.* **23**, 2434–2439.
6. Holmes P, Full RJ, Koditschek D, Guckenheimer J. 2006 The dynamics of legged locomotion: models, analyses, and challenges. *SIAM Rev* **48**, 207–304. (doi:10.1137/S0036144504445133)
7. Floreano D, Ijspeert AJ, Schaal S. 2014 Robotics and neuroscience. *Curr. Biol.* **24**, R910–R920. (doi:10.1016/j.cub.2014.07.058)
8. Ijspeert AJ. 2014 Biorobotics: using robots to emulate and investigate agile locomotion. *Science* **346**, 196–203. (doi:10.1126/science.1254486)
9. Dickinson MH, Lehmann F-O, Sane SP. 1999 Wing rotation and the aerodynamic basis of insect flight. *Science* **284**, 1954–1960. (doi:10.1126/science.284.5422.1954)
10. Ijspeert AJ, Crespi A, Ryczko D, Cabelguen J-M. 2007 From swimming to walking with a salamander robot driven by a spinal cord model. *Science* **315**, 1416–1420. (doi:10.1126/science.1138353)
11. Maladen RD, Ding Y, Li C, Goldman DI. 2009 Undulatory swimming in sand: subsurface locomotion of the sandfish lizard. *Science* **325**, 314–318. (doi:10.1126/science.1172490)
12. Marvi H *et al.* 2014 Sidewinding with minimal slip: snake and robot ascent of sandy slopes. *Science* **346**, 224–229. (doi:10.1126/science.1255718)
13. Libby T, Moore TY, Chang-Siu E, Li D, Cohen DJ, Jusufi A, Full RJ. 2012 Tail-assisted pitch control in lizards, robots and dinosaurs. *Nature* **481**, 181–184. (doi:10.1038/nature10710)
14. Full RJ, Koditschek DE. 1999 Templates and anchors: neuromechanical hypotheses of legged locomotion on land. *J. Exp. Biol.* **202**, 3325–3332.
15. Blickhan R, Full RJ. 1993 Similarity in multilegged locomotion: bouncing like a monopode. *J. Comp. Physiol. A* **173**, 509–517. (doi:10.1007/BF00 197760)
16. Grimes JA, Hurst JW. 2012 The design of ATRIAS 1.0 a unique monopod, hopping robot. In *Proc. Fifteenth Int. Conf. on Climbing and Walking Robots and the Support Technologies for Mobile Machines, Baltimore, MD, USA, July 2012*, pp. 548–554.
17. Saranli U, Buehler M, Koditschek DE. 2001 RHex: a simple and highly mobile hexapod robot. *Int. J. Robot Res.* **20**, 616–631. (doi:10.1177/02783640122067570)
18. Chevallier S, Ijspeert AJ, Ryczko D, Nagy F, Cabelguen J-M. 2008 Organisation of the spinal central pattern generators for locomotion in the salamander: biology and modelling. *Brain Res. Rev.* **57**, 147–161. (doi:10.1016/j.brainresrev.2007.07.006)
19. Ryczko D, Charrier V, Ijspeert AJ, Cabelguen J-M. 2010 Segmental oscillators in axial motor circuits of the salamander: distribution and bursting mechanisms. *J. Neurophysiol.* **104**, 2677–2692. (doi:10.1152/jn.00479.2010)
20. Kragl M, Knapp D, Nacu E, Khattak S, Maden M, Epperlein HH, Tanaka EM. 2009 Cells keep a memory of their tissue origin during axolotl limb regeneration. *Nature* **460**, 60–65. (doi:10.1038/nature08152)
21. Kumar A, Simon A (eds). 2015 *Salamanders in regeneration research. Methods in molecular biology 1290*. New York, NY: Springer.
22. Schaeffer B. 1941 The morphological and functional evolution of the tarsus in amphibians and reptiles. *Bull. Am. Museum Nat. Hist.* **78**, 395–472.
23. Carroll RL. 1988 *Vertebrate paleontology and evolution*. New York, NY: Freeman.
24. Worthington RD, Wake DB. 1972 Patterns of regional variation in the vertebral column of terrestrial salamanders. *J. Morphol.* **137**, 257–277. (doi:10.1002/jmor.1051370302)
25. Romer AS, Byrne F. 1931 The pes of *Diadectes*: notes on the primitive tetrapod limb. *Palaeobiologica* **4**, 25–48.
26. Howell AB. 1944 *Speed in animals*. New York, NY: Hafner Publishing Company.
27. Barclay OR. 1946 The mechanics of amphibian locomotion. *J. Exp. Biol.* **23**, 177–203.
28. Gray J. 1968 *Animal locomotion*. London, UK: Weidenfeld & Nicolson.
29. Edwards JL. 1989 Two perspectives on the evolution of the tetrapod limb. *Am. Zool.* **29**, 235–254. (doi:10.1093/icb/29.1.235)
30. Gao K-Q, Shubin NH. 2001 Late Jurassic salamanders from northern China. *Nature* **410**, 574–577. (doi:10.1038/35069051)
31. Clack JA. 2002 An early tetrapod from 'Romer's gap'. *Nature* **418**, 72–76. (doi:10.1038/nature00824)
32. Petti FM, Bernardi M, Ashley-Ross MA, Berra F, Tessarollo A, Avanzini M. 2014 Transition between terrestrial-submerged walking and swimming revealed by Early Permian amphibian trackways and a new proposal for the nomenclature of compound trace fossils. *Palaeogeogr. Palaeoclimatol. Palaeoecol.* **410**, 278–289. (doi:10.1016/j.palaeo.2014.05.032)
33. Knüsel J, Bicanski A, Ryczko D, Cabelguen J-M, Ijspeert AJ. 2013 A salamander's flexible spinal network for locomotion, modeled at two levels of abstraction. *Integr. Comp. Biol.* **53**, 269–282. (doi:10.1093/icb/ict067)
34. Crespi A, Karakasiliotis K, Guignard A, Ijspeert AJ. 2013. Salamandra robotica II: an amphibious robot to study salamander-like swimming and walking gaits. *IEEE Trans. Robot.* **29**, 308–320. (doi:10.1109/TRO.2012.2234311)
35. Ashley-Ross MA. 1994 Hindlimb kinematics during terrestrial locomotion in a salamander (*Dicamptodon tenebrosus*). *J. Exp. Biol.* **193**, 255–283.
36. Karakasiliotis K, Schilling N, Cabelguen J-M, Ijspeert AJ. 2012 Where are we in understanding salamander locomotion: biological and robotic perspectives on kinematics. *Biol. Cybern.* **107**, 529–544. (doi:10.1007/s00422-012-0540-4)
37. Karakasiliotis K, Ijspeert AJ. 2009 Analysis of the terrestrial locomotion of a salamander robot. In *IEEE/RSJ Int. Conf. Intelligent Robots and Systems, 2009*. IROS 2009, pp. 5015–5020.
38. Fischer MS, Lehmann R. 1998 Application of cineradiography for the metric and kinematic study of in-phase gaits during locomotion of the pika (*Ochotona rufescens*, Mammalia: Lagomorpha). *Zoology* **101**, 148–173.
39. Brainerd EL, Baier DB, Gatesy SM, Hedrick TL, Metzger KA, Gilbert SL, Crisco JJ. 2010 X-ray reconstruction of moving morphology (XROMM): precision, accuracy

and applications in comparative biomechanics research. *J. Exp. Zool. Part A. Ecol. Genet. Physiol.* **313**, 262–279. (doi:10.1002/jez.589)

40. Andrada E, Mämpel J, Schmidt A, Fischer MS, Witte H. 2013 From biomechanics of rats' inclined locomotion to a climbing robot. *Int. J. Des. Nat. Ecodyn*. **8**, 191–212. (doi:10.2495/DNE-V8-N3-192-212)
41. El Daou H, Libourel P-A, Renoust S, Belst V, Guinot J-C. 2010 *Motion and force measures on tortoises to design and control a biomimetic quadruped robot*. Berlin, Germany: Springer.
42. Delvolvé I, Branchereau P, Dubuc R, Cabelguen J-M. 1999 Fictive rhythmic motor patterns induced by NMDA in an *in vitro* brain stem–spinal cord preparation from an adult urodele. *J. Neurophysiol.* **82**, 1074–1077.
43. Delvolvé I, Bem T, Cabelguen J-M. 1997 Epaxial and limb muscle activity during swimming and terrestrial stepping in the adult newt, *Pleurodeles waltl*. *J. Neurophysiol.* **78**, 638–650.
44. Karakasiliotis K. 2013 Legged locomotion with spinal undulations. PhD thesis, École polytechnique fédérale de Lausanne EPFL.
45. Taylor GK, Nudds RL, Thomas ALR. 2003 Flying and swimming animals cruise at a Strouhal number tuned for high power efficiency. *Nature* **425**, 707–711. (doi:10.1038/nature02000)
46. Spence AJ. 2009 Scaling in biology. *Curr. Biol.* **19**, R57–R61. (doi:10.1016/j.cub.2008.10.042)
47. Alexander RM. 2003 *Principles of animal locomotion*. Princeton, NJ: Princeton University Press.
48. Alexander RM. 1984 Walking and running: legs and leg movements are subtly adapted to minimize the energy costs of locomotion. *Am. Sci.* **72**, 348–354.
49. Gatesy SM, Biewener AA. 1991 Bipedal locomotion: effects of speed, size and limb posture in birds and humans. *J. Zool.* **224**, 127–147. (doi:10.1111/j.1469-7998.1991.tb04794.x)
50. Moretto P, Pelayo P, Lafortune MA. 1996 The use of Froude's numbers to normalize human gait. In *Proc. The Ninth Biennial Conf. And Symposia: Simon Fraser University, 22–24 August, Burnaby, Canada*, p. 274.
51. Burcher R, Rydill LJ. 1998 *Concepts in submarine design*. The press syndicate of the University of Cambridge. Cambridge, UK: Cambridge University Press.
52. Moonesun M, Javadi M, Charmdooz P, Mikhailovich KU. 2013 Evaluation of submarine model test in towing tank and comparison with CFD and experimental formulas for fully submerged resistance. *Indian J. Geo-Mar. Sci.* **42**, 1049–1056.
53. Johansson LC, Lauder GV. 2004 Hydrodynamics of surface swimming in leopard frogs (*Rana pipiens*). *J. Exp. Biol.* **207**, 3945–3958. (doi:10.1242/jeb.01258)
54. Hoerner SF. 1965 *Fluid-dynamic drag: practical information on aerodynamic drag and hydrodynamic resistance*. Midland Park, NJ: Hoerner Fluid Dynamics.
55. Gillmer TC. 2012 *Introduction to naval architecture*. Berlin, Germany: Springer Science & Business Media.
56. Heglund NC, Taylor CR, McMahon TA. 1974 Scaling stride frequency and gait to animal size: mice to horses. *Science* **186**, 1112–1113. (doi:10.1126/science.186.4169.1112)
57. Crespi A, Ijspeert AJ. 2008 Online optimization of swimming and crawling in an amphibious snake robot. *IEEE Trans. Robot.* **24**, 75–87. (doi:10.1109/TRO.2008.915426)
58. D'Août K, Aerts P. 1997 Kinematics and efficiency of steady swimming in adult axolotls (*Ambystoma mexicanum*). *J. Exp. Biol.* **200**, 1863–1871.
59. Kawano SM, Blob RW. 2013 Propulsive forces of mudskipper fins and salamander limbs during terrestrial locomotion: implications for the invasion of land. *Integr. Comp. Biol.* **53**, 283–294. (doi:10.1093/icb/ict051)
60. Aguilar J *et al.* 2016 A review on locomotion robophysics: the study of movement at the intersection of robotics, soft matter and dynamical systems. (arXiv:1602.04712).
61. Miranda DL, Rainbow MJ, Crisco JJ, Fleming BC. 2013 Kinematic differences between optical motion capture and biplanar videoradiography during a jump–cut maneuver. *J. Biomech.* **46**, 567–573. (doi:10.1016/j.jbiomech.2012.09.023)
62. Spröwitz A, Tuleu A, Vespignani M, Ajallooeian M, Badri E, Ijspeert AJ. 2013 Towards dynamic trot gait locomotion: design, control, and experiments with Cheetah-cub, a compliant quadruped robot. *Int. J. Robot Res.* **32**, 932–950. (doi:10.1177/0278364913489205)
63. Ding Y, Sharpe SS, Wiesenfeld K, Goldman DI. 2013 Emergence of the advancing neuromechanical phase in a resistive force dominated medium. *Proc. Natl Acad. Sci. USA* **110**, 10 123–10 128. (doi:10.1073/pnas.1302844110)
64. Tsagarakis NG, Morfey S, Cerda GM, Zhibin L, Caldwell DG. 2013 Compliant humanoid coman: optimal joint stiffness tuning for modal frequency control. In *2013 IEEE Int. Conf. on Robotics and Automation* (*ICRA*), *6–10 May, Karlsruhe, Germany*, pp. 673–678. IEEE.
65. Pratt G, Williamson MM. 1995 Series elastic actuators. In *Intelligent Robots and Systems 95. 'Human Robot Interaction and Cooperative Robots', Proc. 1995 IEEE/RSJ Int. Conf., 5–9 August, Pittsburgh, PA*, vol. 1, pp. 399–406. IEEE.
66. Cheng J, Stein RB, Jovanovic K, Yoshida K, Bennett DJ, Han Y. 1998 Identification, localization, and modulation of neural networks for walking in the mudpuppy (*Necturus maculatus*) spinal cord. *J. Neurosci.* **18**, 4295–4304.